Novel Process for Screen-Printed Selective Area Front Polysilicon Contacts for TOPCon Cells Using Laser Oxidation

Sagnik Dasgupta, Young-Woo Ok, Vijaykumar D. Upadhyaya, Wook-Jin Choi, Ying-Yuan Huang, Shubham Duttagupta, and Ajeet Rohatgi

***Abstract*—The efficiency potential of double-side tunnel oxide passivated contact (DS-TOPCon) solar cells is limited by parasitic absorption in the front poly-Si layer, despite excellent passivation and high V_{OC}. The use of patterned poly-Si only under the front metal grid lines can significantly reduce the parasitic absorption loss without sacrificing voltage. In this work, we demonstrate a simple, manufacturing-friendly method of patterning the front poly-Si using a nanosecond UV (355 nm) laser. We found that with laser powers $\geq$3 W at a 400 mm/s scan speed, an estimated 1–4 nm thick stoichiometric SiO_2 layer was grown on TOPCon. This served as a mask for KOH-etching of 200 nm poly-Si, allowing for patterning of poly-Si fingers required for selective TOPCon. While laser powers above 3 W caused substantial deterioration in passivation quality, the resulting damage in J_0 was largely recovered by subsequent PECVD SiN_x deposition. At 3 W, the full area J_0 was found to be 36.8 fA·cm^{-2}. This translates to 1.68 fA·cm^{-2} for 4.48% coverage from the wing area of the polyfinger lines (100 lines–100 μm wide and 30 μm metal) contributing to a total front J_0 of $\sim$10 fA·cm^{-2}, well suited for 25% efficient solar cells.**

***Index Terms*—Double-side TOPCon, laser oxidation, passivating contacts, screen-printed contacts, selective area contacts.**

I. Introduction

THE vast majority of commercial crystalline silicon solar cells use phosphorus diffused emitters/junctions on the front side that limit the efficiency by the heavily doped regions and metal-induced recombination at the contacts. Carrier-selective passivating contacts can mitigate this loss by displacing the diffused and metalized regions outside the Si wafer and providing appropriate band bending for collecting carriers while preventing minority carrier recombination at the metal–semiconductor and oxide–semiconductor interfaces. Tunnel oxide passivated contacts (TOPCon) utilize an ultrathin tunneling SiO_2 layer capped with doped poly-Si to provide passivation and carrier selectivity, respectively [1]. TOPCon-based cells have the added benefit of being compatible with traditional fire-through screen-printed metallization, making them compatible with preexisting solar cell production lines. While having full-area poly-Si contacts on both sides of a solar cell can yield V_{OC} as high as 728 mV [2], using thick poly-Si on the front of a solar cell, results in significant current loss due to parasitic light absorption. On the other hand, thinning the front poly-Si increases damage during fire-through metallization and leads to higher J_0 [3]. This has restricted the use of TOPCon only on the rear side of the screen-printed solar cell utilizing a traditionally diffused front junction with record efficiencies around 25% [4].

Using a patterned TOPCon only under the metal grid on the front can significantly reduce parasitic absorption and boost cell efficiency [5]. Moreover, for rear-junction solar cells, efficiency is nearly independent of front sheet resistance, allowing for the use of polyfingers or selective area front TOPCon with a dielectric passivated undiffused Si wafer in the field region. This concept works because for this cell design with appropriate bulk resistivity and lifetime carrier transport on the front side occurs through bulk Si without appreciable resistive loss [6]. This can be accomplished by forming a patterned mask on the full area poly-Si, etching the poly-Si in the field region around the mask to define polyfingers, and stripping the mask before metallization. A schematic of a solar cell based on this design is shown in Fig. 1. This process can be cumbersome and expensive and may reduce yield if done by conventional methods [7]. Alternatively, Chen et al. [8], used a self-aligned metal mask and TMAH etching to create such a device. However, their process involves thermally evaporated metal, which is not suitable for industrial use. In this article, we reveal a simple, manufacturable, clean, and rapid process involving laser oxidation to fabricate selective TOPCon on the front side of a solar cell.

In this work, we demonstrate the use of a pulsed ultraviolet (UV) nanosecond laser to form a patterned oxide to serve as a poly-Si etch mask on the full area TOPCon. We show that at certain power densities of our UV laser it is possible to

Manuscript received 30 May 2022; revised 23 July 2022; accepted 29 July 2022. Date of publication 29 August 2022; date of current version 28 November 2022. This work was supported by the U.S. Department of Energy's Office of Energy Efficiency and Renewable Energy through Solar Energy Technologies Office Agreement under Grant DE-EE0009350, Grant DE-EE0008562, and Grant DE-EE0008975. *(Corresponding author: Sagnik Dasgupta.)*

Sagnik Dasgupta, Young-Woo Ok, Vijaykumar D. Upadhyaya, Wook-Jin Choi, and Ajeet Rohatgi are with the Georgia Institute of Technology, Atlanta, GA 30332 USA (e-mail: sdasgupta@gatech.edu; yok6@mail.gatech.edu; kumar@ece.gatech.edu; wookjin4686@gatech.edu; ajeet.rohatgi@ece.gatech.edu).

Ying-Yuan Huang is with the Georgia Institute of Technology, Atlanta, GA 30332 USA, and also with the College of Photonics, National Yang Ming Chiao Tung University, Tainan 71150, Taiwan (e-mail: yingyuanhuang@gatech.edu).

Shubham Duttagupta is with the Solar Energy Research Institute of Singapore, The National University of Singapore, Singapore 117574 (e-mail: shubham.duttagupta@nus.edu.sg).

Color versions of one or more figures in this article are available at https://doi.org/10.1109/JPHOTOV.2022.3196822.

Digital Object Identifier 10.1109/JPHOTOV.2022.3196822

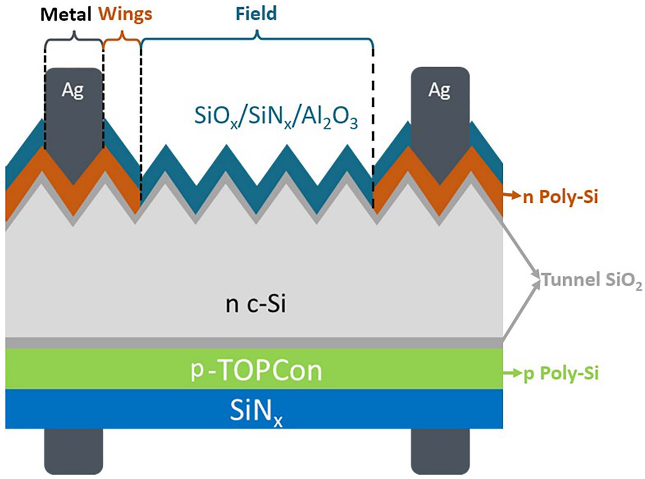

Fig. 1. Schematic of a rear junction selective area double side TOPCon solar cell. The metallization is only performed on selectively etched fingers of polysilicon, enabling excellent light transparency in the field region.

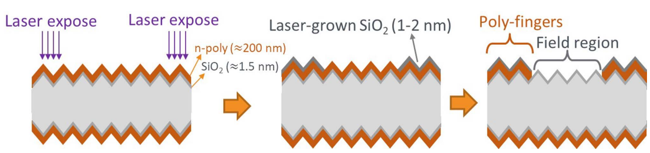

Fig. 2. General process flow for laser-grown oxide mask patterning and subsequent poly-Si etching.

grow a very thin (few nm thick) silicon oxide layer that is sufficient to prevent etching of the underlying poly-Si during the poly-Si etch between the finger pattern. Schäfer et al. [9] used a picosecond laser to achieve similar etch-masking behavior. However, due to significantly lower power densities involved, their etch resistance, while assisted by oxygen, was attributed to amorphization of the surface of the poly-Si [10].

II. Fabrication and Characterization of TOPCon Symmetric Structures

Symmetric n-poly-Si/SiO_2/n-Si/SiO_2/n-poly-Si test structures were grown on $\sim$3 Ω·cm n-type Cz-Si wafers textured on both sides with random pyramids. Tunnel oxide was grown using the NAOS process [11] on both sides of the wafers in HNO_3 at 100 °C for 15 min, resulting in a thickness of about 15 Å. Subsequently, $\sim$200 nm n-type poly-Si was grown in a Tystar LPCVD tube at 588 °C. Test samples for sheet resistance measurements were made with the same process on p-type wafers. Layers for optical measurements were grown on polished CZ wafers with 150 nm of PECVD SiO_x for better ellipsometry.

A. UV Laser Patterning

Fig. 2 shows a schematic of the laser patterning process. First, the poly-Si coated wafer was patterned to define grid lines with laser irradiation from a Coherent Avia 355-10 nanosecond pulsed UV laser (355 nm) as a function of laser power controlled by the pulse repetition frequency. All laser scans were performed at 400 mm/s with a spot size of 70 µm. After patterning, the wafers were immersed in 9%$_{vol}$ KOH at 40 °C to remove the poly-Si from the field region, resulting in patterned poly-Si fingers. For lifetime test structures, laser patterning was only done on one side of the wafer. Subsequently, $\sim$70 nm of SiN_x was deposited at a temperature of 450 °C and at a pressure of 1700 mtorr for 700 s on both sides of the samples in a Centrotherm PECVD reactor to mimic the SiN_x required for the fire-through screen-printed contact process. The objective is to define 100–150 µm wide poly-Si fingers/TOPCon on top of which 30–40 µm screen-printed metal fingers will be formed and aligned by an industrial-compatible screen-printing process.

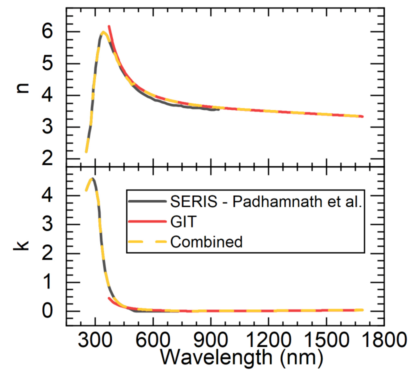

Fig. 3. Combined refractive index (n) and extinction coefficient (k) obtained from measurements at Georgia Tech (this work) and by Padhamnath et al. [14].

B. Measurements

Optical constants of the grown poly-Si layers were obtained through spectroscopic ellipsometry measurements on a J.A. Woollam M-2000 ellipsometer. Carrier lifetimes J_0 and iV_{oc} of the n-type test structures were measured by photoconductance decay measurement using a Sinton WCT-120. Sheet resistances on the n-poly-Si/SiO_2/p-Si/SiO_2/n-poly-Si structures were measured using a four-point probe. Further, the laser-grown oxide was characterized using a Thermo K-alpha XPS. Surface morphologies of the laser-processed samples were observed using a laser scanning confocal microscope (Keyence VK-X3000).

III. Results and Discussion

A. Optical Modeling of Selective Area Front Polysilicon Solar Cells

For accurate optical modeling, the refractive index and extinction coefficient of the grown n-poly-Si were obtained through spectroscopic ellipsometry. The raw data were fit to two Tauc–Lorentz oscillators [12] to account for visible range absorption and a Drude oscillator [13] for free carrier absorption in the near IR range. Due to limitations of the ellipsometer, measurements are made between 370 and 1687 nm. However, for a poly-Si layer at the front of a solar cell, quantifying UV range absorption is crucial. As shown in Fig. 3, in the range between 400 and

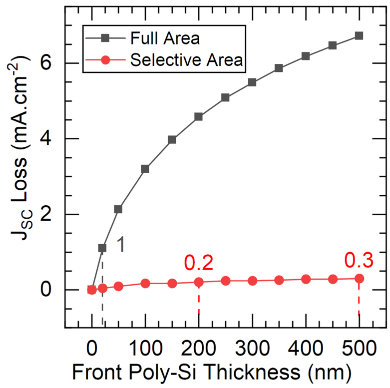

Fig. 4. Simulated J_{SC} loss due to parasitic absorption of light in the front poly-Si for full area and selective TOPCon structures.

700 nm, our optical constants are very similar to those measured by Padhamnath et al. [14]. Therefore, for optical modeling, Padhamnath's data were used between 250 and 500 nm, and our measurements were utilized in the remaining wavelength range.

The refractive index and extinction coefficient data discussed previously were used in PVLighthouse's OPAL 2 optical simulation program [15], [16] to model the parasitic absorption of light in the front poly-Si similar to a process described by Huang et al. [5]. For full-area front TOPCon, the parasitic absorption in poly-Si ($J_{\text{abs, Poly}}$) can be calculated as the difference of generated current in the absorber with ($J_{\text{gen, Poly}}$) and without ($J_{\text{gen, NoPoly}}$) poly-Si, given as follows:

$$J_{\text{abs, Poly}} = J_{\text{gen, NoPoly}} - J_{\text{gen, Poly}}. \tag{1}$$

For 100 µm wide poly-Si fingers at a pitch of 1.56 mm shaded with 30 µm metal lines at the front of a solar cell, the total area of poly-Si exposed to light is 4.48%. The component of the generated current absorbed in this "wing area" is given as follows:

$$J_{\text{abs,Wing}} = J_{\text{abs, Poly}} \times 4.48\% \tag{2}$$

Therefore, the generation current in such a selective TOPCon structure can be quantified as follows:

$$J_{\text{gen,Selective}} = J_{\text{gen, NoPoly}} - J_{\text{abs,wing}} \tag{3}$$

From these equations, it is inferred that the loss in J_{SC} in selective and full area font TOPCon cells are approximately equal to $J_{\text{abs,Wing}}$ and $J_{\text{abs,Poly}}$, respectively. Fig. 4 shows the simulated J_{SC} loss as a function of front poly-Si thickness for both full area and selective area TOPCon. We find that exceeding 20 nm of full area poly-Si on the front of the solar cell will incur a current loss over 1 mA·cm^{-2}. On the other hand, using a selective TOPCon structure renders the front parasitic absorption far less sensitive to the thickness of the poly-Si. For 200-nm thick selective poly-Si fingers, only 0.2 mA·cm^{-2} current density is lost in poly-Si, allowing for easy and high-quality fire-through screen-printed metallization. In fact, increasing the thickness by a factor of 2.5–500 nm results in a loss of only an additional 0.1 mA·cm^{-2}, indicating that the current loss in this device structure is very forgiving to the increased poly-Si thickness while potentially improving passivation quality (lower J_0) with fire-through screen-printed contacts [3].

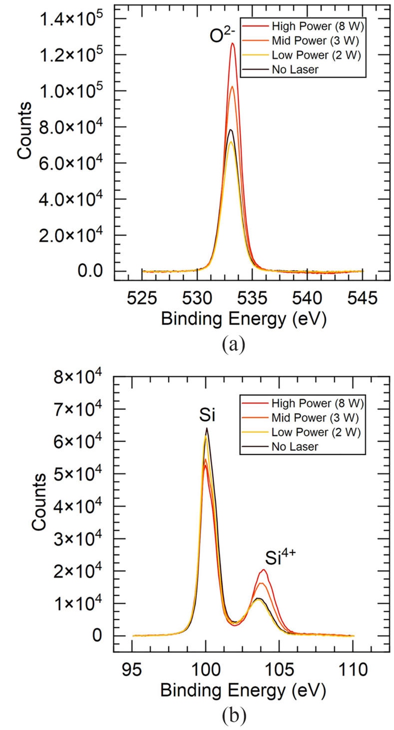

Fig. 5. (a) O^{2-} and (b) Si^{4+} peaks on XPS for various laser powers. Higher laser powers grow thicker and more stoichiometric oxides at a given scan speed.

B. Laser-Induced Oxidation of Polysilicon

XPS measurements in Fig. 5(a) show an increase in the intensity of the divalent oxygen peak (O^{2-}) at 532 eV, which, in our case, is related to the thickness of surface SiO_2 present [17]. This demonstrates growth of silicon oxide with the UV laser and shows that increased laser power increases the oxide thickness beyond that of native oxide. Laser-grown oxide thickness is estimated to be in the range of 1–4 nm. Moreover, the shift in the Si^{4+} peak (at 103.5 nm) in Fig. 5(b) indicates that laser oxide is more stoichiometric than the native oxide [18]. This suggests that the oxide growth mechanism is similar to thermal oxidation as governed by the Deal–Grove model. Similar observations on oxidation with a nanosecond UV laser were made by Orlowski et al. [19].

C. Demonstration of Laser Oxide As Etch Mask

We used a 9%$_{\text{vol}}$ KOH solution (DI water:45% KOH ≡ 5:1) at 40 °C to etch poly-Si between the laser patterned oxide to form poly-Si fingers. This solution is highly selective in etching silicon over SiO_x. It was observed that 200 nm of poly-Si can be etched at 40 °C in ∼90 s. In addition, the laser-grown oxide

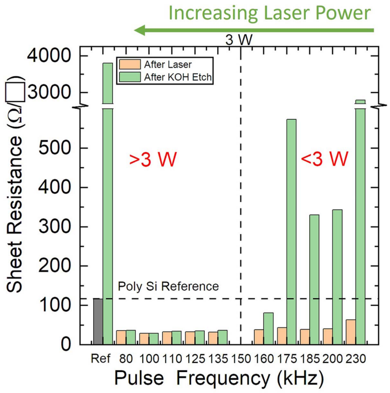

Fig. 6. Measured sheet resistance of Poly-Si films before and after KOH etch. For laser powers greater than 3 W, the sheet resistance does not change with KOH etching, indicating protection of the poly-Si by the laser grown oxide.

was successful in preventing etching of the underlying poly-Si, serving as an effective etching mask to form polyfingers.

The presence of poly-Si after 2 min of KOH immersion was verified through sheet resistance measurement of 25 mm square lasered areas on the n-type poly-Si films grown on p-type wafers, as shown in Fig. 6. Without any laser treatment, the poly-Si showed a sheet resistance of 120 Ω/□. After two min of KOH etching, this increased to ∼3800 Ω/□ indicating complete removal of poly-Si. For all tested laser powers, the sheet resistance decreased significantly to ∼30 Ω/□ after laser treatment. This suggests a laser-induced change in surface dopant concentration of the deposited poly-Si. More importantly, for powers over 3 W (pulse frequencies below 150 kHz), the sheet resistance does not change before and after 2 min of KOH poly-Si etch, demonstrating successful protection of the phosphorus doped poly-Si layer under the laser-grown oxide. Conversely, at powers below 3 W, we observed that the post-etch sheet resistance increased, indicating thinning of the poly-Si layer. Therefore, below 3 W of laser power, the oxide grown by the laser, if any, was inadequate to protect the doped layer from KOH etching.

D. Laser-Induced Surface Damage, Degradation of Passivation, and Its Recovery By Subsequent SiN_x Deposition

Fig. 7 shows laser confocal micrographs of the textured surface of a silicon wafer at different laser powers. Compared with the reference textured wafer, the sample at 8 W shows significant rounding of pyramids. At 3 W of laser power, while the damage is less, there is still observable rounding of the tips of the pyramids. Change in the morphology of the 3–5 μm sized pyramids implies that the damage depth of the laser exceeds the thickness of the poly-Si. This suggests that the recombination at the Si/SiO_x/Poly-Si interface would be affected by the laser.

The passivation of the absorber is quantified using J_0 obtained from photoconductance measurements (Table 1). For the reference (not lasered) sample, the measured total J_0 of the as deposited symmetric TOPCon test structure was 64.5 fA·cm^{-2}, which was reduced to 12.8 fA·cm^{-2} after deposition of 70 nm PECVD SiN_x on both sides. Since this is a symmetric structure, $J_{0,\,\mathrm{poly}} = 6.4$ fA·cm^{-2} for each surface.

TABLE I
STRUCTURE J_0 WITH DIFFERENT LASER POWERS

Laser Power	J_0 (Both Sides)		
	No Laser	After Laser	After SiN_x Deposition
Reference	64.5 fA·cm^{-2}	-	12.8 fA·cm^{-2}
1.8 W	-	518 fA·cm^{-2}	15.8 fA·cm^{-2}
3 W	-	1860 fA·cm^{-2}	43.2 fA·cm^{-2}
8 W	-	2309 fA·cm^{-2}	194 fA·cm^{-2}

Fig. 8 shows that laser oxidation caused significant deterioration in passivation increasing the measured total J_0 values in the range of 500–2300 fA·cm^{-2}. However, after the subsequent SiN_x deposition, which is required for screen-printed metallization, the J_0 value decreased dramatically from 15 fA·cm^{-2} at 1.8 W to 194 fA·cm^{-2} at 8 W. No further change was observed after belt furnace firing without screen-printed metal at a peak temperature of 760 °C.

This improvement is likely due to hydrogenation of the surface resulting from the nitride growth [20]. At 3 W of laser power, above which the laser-grown oxide acts as an etch mask, the J_0 of the test structure was 43.2 fA·cm^{-2} after SiN_x deposition. Since the laser treatment was performed only on one side of the wafer, the J_0 of the lasered surface can be obtained by subtracting the J_0 of the nonlasered surface from the total J_0, giving us 36.8 fA·cm^{-2} for the laser-treated surface. However, this translates into only 1.65 fA·cm^{-2} for J_0 contribution from the unmetallized wings of polyfingers because of 4.48% area coverage on the front of the solar cell.

E. Device Simulations of Laser Processed Selective TOPCon

The efficiency potential of the cell structure shown in Fig. 1 was studied through 2-D device simulations in Quokka 2 [21]. The parameters used in the model are detailed in Table II. The J_0 of the wing areas of the polyfingers was approximated to 40 fA·cm^{-2} based on the discussion in Section III-D. Furthermore, with the increasing popularity of busbarless solar cells and measurement methods, we have adopted that design in our simulations [22]. The device characteristics for this simulated solar cell are shown in Fig. 9 with efficiency approaching 25%. Using this model as a baseline, the dependence of performance on various inputs is studied in the next sections.

1) Dependence of Solar Cell Performance on Polyfinger Thickness: Fig. 10(a) shows the efficiency of the solar cell as a function of thickness of the front selective poly-Si under the metal fingers. As suggested by our OPAL 2 model discussed in Section III-A, the J_{sc} and hence the efficiency of a selective area front TOPCon structure, is relatively insensitive to the thickness of the poly-Si. In fact, we observe that increasing the thickness from 200–500 nm incurs only an additional 0.05% loss in absolute efficiency, potentially allowing less damaging metallization without incurring a significant drop in current.

2) Dependence of Solar Cell Performance on Polyfinger Width: Polyfinger width affects device performance in two ways: (1) wider polyfingers incur higher current loss due to parasitic light absorption in the wing area and (2) increased contribution of the $J_{0.\mathrm{FrontPoly}}$ to the total J_0. Because the

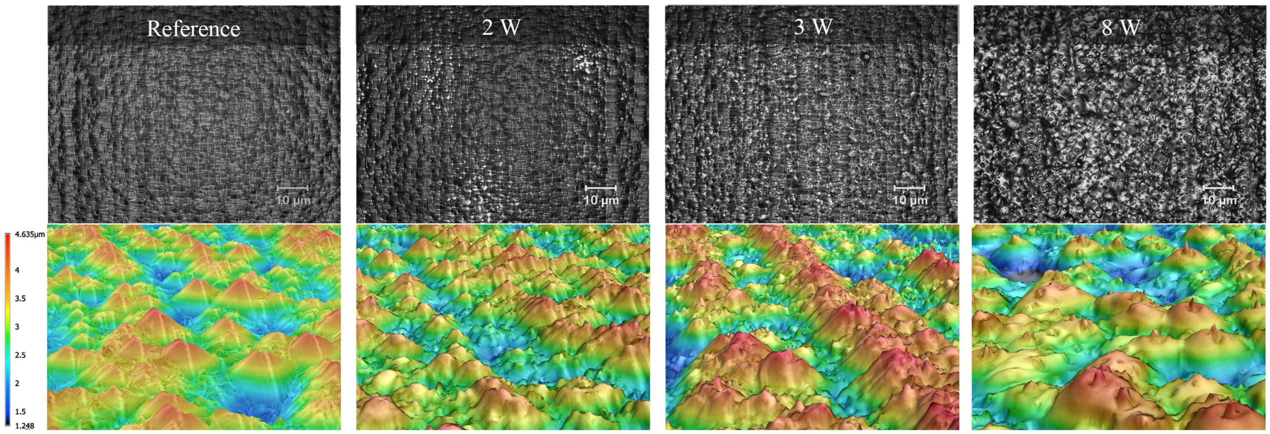

Fig. 7. Laser confocal microscopy images in plan view and isometric view showing increasing damage to the surface morphology at higher laser powers.

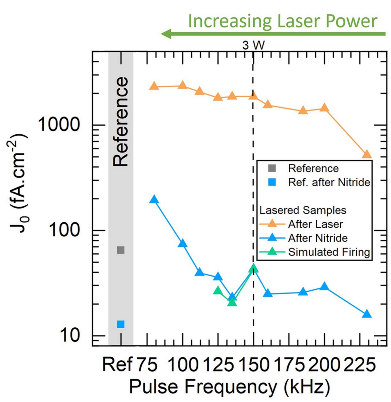

Fig. 8. Deterioration of J_0 after laser incidence and subsequent recovery of passivation after SiN_x deposition.

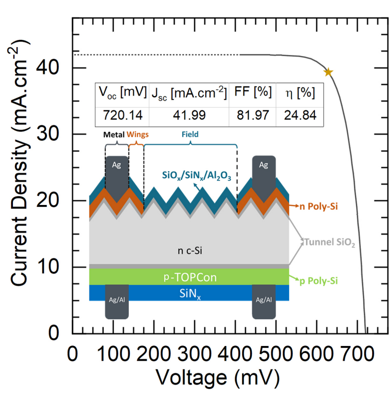

Fig. 9. Current–voltage characteristics of the simulated selective-front double-side TOPCon solar cell.

TABLE II
INPUT PARAMETERS FOR QUOKKA 2 DEVICE SIMULATION

	Parameter	Value	Reference
Cell Data	**V_{OC} [mV]**	**720.15**	
	J_{SC} [mA·cm^{-2}]	**41.99**	
	FF [%]	**81.98**	
	Efficiency [%]	**24.84**	
	Total J_0 [fA·cm^{-2}]	**34**	
Front Selective TOPCon	Front Poly Type	N (textured)	
	Selective area width [μm]	100 **(variable)**	
	Front Poly thickness [nm]	200 **(variable)**	
	Front field SRV [cm/s]	3.8	[23]
	$J_{0frontpoly,pass}$ [fA·cm^{-2}]	40	Section III-D
	$J_{0frontpoly,metal}$ [fA·cm^{-2}]	300 **(variable)**	In house
	$J_{0front,total}$ [fA·cm^{-2}]	**12**	
Bulk	Bulk Type	N	
	Bulk thickness [μm]	170	
	Bulk resistivity [Ω-cm]	1	[5]
	SRH τ_{n0}[ms]	5	[5]
	SRH τ_{p0}[ms]	5	[5]
	$J_{0bulk,total}$ [fA·cm^{-2}]	**11**	
Rear TOPCon	Rear Poly Type	P (planar)	
	Rear Poly thickness [nm]	200	
	Rear Poly sheet resistance [Ω/□]	200	In house
	$J_{0rearpoly,pass}$ [fA·cm^{-2}]	4.6	[24]
	$J_{0rearpoly,metal}$ [fA·cm^{-2}]	112	[24]
	$J_{0rear,total}$ [fA·cm^{-2}]	**11**	
Front grid	Number of lines	100	
	Pitch [mm]	1.56	
	Line thickness [μm]	30	
	Metal coverage	1.92%	
	Contact resistivity [mΩ·cm²]	2 **(variable)**	[25]
Rear grid	Number of lines	200	
	Pitch [mm]	0.78	
	Line thickness [µm]	30	
	Metal coverage	3.84%	
	Contact resistivity [mΩ·cm²]	3	[24]
	External Rs [Ω-cm²]	0.009	
	Jgen [mA/cm²]	43.26	Section III.A

$J_{0.\mathrm{FrontPoly}}$ is significantly higher than $J_{0,\mathrm{field}}$ ($= 5$ fA·cm^{-2} calculated from SRV of 3.8 cm·s^{-1}) due to laser damage, increasing the width causes deterioration in V_{OC}. However, due to the low overall area fraction, the effect of this deterioration is diminished. We observe that doubling the width from 100 to 200 µm decreases the V_{OC} by 2.1 mV and the J_{SC} by 0.4 mA·cm^{-2}, together amounting to an efficiency loss of only 0.2%, as shown in Fig. 10(b). This can help relax the metal grid alignment requirements if needed.

3) Dependence of Performance on $J_{0,metal}$ on the Front of the Solar Cell: The reference simulation above uses $J_{0,\mathrm{metal}-100\%} = 300$ fA·cm^{-2}. This was obtained through initial experiments on laser-processed symmetric n-TOPCon samples based on the methodology described by Huang et al. [26]. For

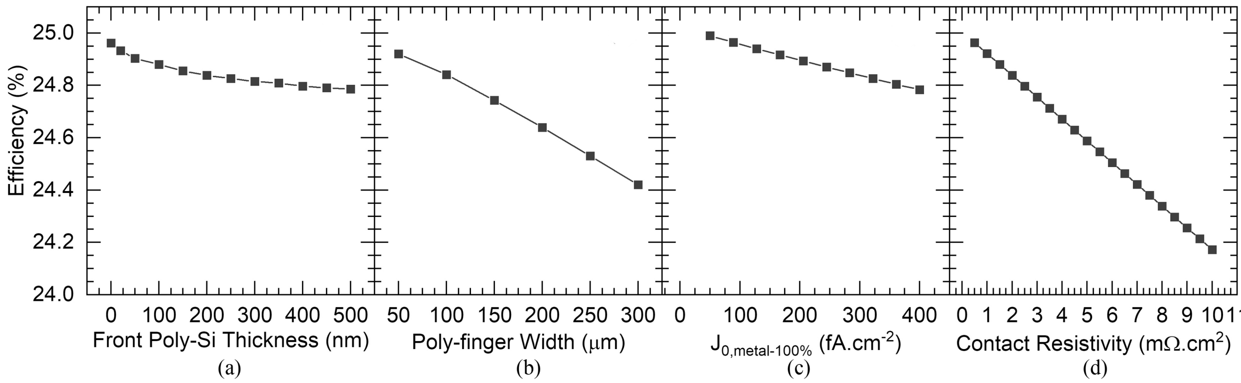

Fig. 10. Variation of simulated solar cell efficiency as a function of (a) polyfinger thickness, (b) polyfinger width, (c) $J_{0,\mathrm{metal}}$, and (d) contact resistivity.

30 μm wide metal lines, amounting to a coverage fraction of 1.92%, this amounts to an effective contribution of 5.76 fA·cm^{-2}. Fig. 10(c) shows that decreasing the full area $J_{0,\mathrm{metal}}$ from 300 – 50 fA·cm^{-2} (0.96 fA·cm^{-2} for 1.92% metal coverage) can increase the efficiency of the cell from 24.84% to 25%. This shows that when the metal coverage is low, the efficiency does not vary significantly with $J_{0,\mathrm{metal}}$.

4) Dependence of Performance on Contact Resistivity of Metal/TOPCon Stack: For optimally metalized high-quality n-TOPCon layers, achieving a contact resistivity of 2 mΩ·cm^2 is not uncommon [25], [27]. However, low temperature or underfiring of the metallization can increase contact resistivities. The simulations show that for this cell structure every 2 mΩ·cm^2 increase in contact resistivity decreases the fill factor by ∼0.5% and the efficiency by ∼0.2%. This dependence is shown in Fig. 10(d).

IV. Conclusion

In this work, we have demonstrated the growth of 1–4 nm silicon oxide on TOPCon using a 355-nm nanosecond UV laser. We have shown that for laser powers above 3 W at 400 mm/s, the grown oxide layer can protect the underlying selective TOPCon from KOH etching. Despite the appreciable degradation in J_0 from the laser treatment, passivation quality is largely recovered after subsequent PECVD SiN_x deposition, which is required for screen printed contacts. At 3 W of laser power, a full area J_0 of 36.8 fA·cm^{-2} was achieved, which translates to only 1.65 fA·cm^{-2} for 4.48% coverage of polyfingers (100 polyfingers, 100 μm wide, and with 30 μm of metal). Based on our Quokka 2 modeling of double-side TOPCon cells with selective area poly-Si on the front with practically achievable material parameters, the performance of a back junction bifacial fully screen-printed solar cell can approach 25%. Further, we have found that a front selective area poly-Si-based solar cell is very insensitive to the passivation quality of the front contact. These advantages combined with the ease of fabricating this selective area front TOPCon structure using the novel laser-oxide patterning technology make it a strong contender for the next generation of high-efficiency silicon solar cells.

Acknowledgment

The authors would like to thank Mr. Richard Shafer for consistent assistance in the operation of the laser system used in this work and Mr. Walter Henderson for the XPS measurements.

References

[1] F. Feldmann et al., “Tunnel oxide passivated contacts as an alternative to partial rear contacts,” *Sol. Energy Mater. Sol. Cells*, vol. 131, pp. 46–50, Dec. 2014, doi: 10.1016/j.solmat.2014.06.015.

[2] Y. Larionova et al., “Ultra-thin poly-SI layers: Passivation quality, utilization of charge carriers generated in the poly-si and application on screen-printed double-side contacted polycrystalline SI on oxide cells,” *Sol. RRL*, vol. 4, no. 10, 2020, Art. no. 2000177, doi: 10.1002/solr.202000177.

[3] F. Feldmann et al., “Industrial TOPCon solar cells realized by a PECVD tube process,” in *Proc. 37th Eur. PV Sol. Energy Conf. Exhib.*, 2020, vol. 7, pp. 7–11. doi: 10.4229/EUPVSEC20202020-2AO.6.3.

[4] “JinkoSolar: ‘Record’ 25.25% efficiency for TOPCon cell | taiyangnews,” Accessed: Jul. 19, 2022. [Online]. Available: https://taiyangnews.info/technology/jinkosolar-record-25-25-efficiency-for-n-type-mono-cell/

[5] Y.-Y. Huang et al., “Modeling and understanding of rear junction double-side passivated contact solar cells with selective area TOPCon on front,” in *Proc. IEEE 48th Photovolt. Specialists Conf.*, 2021, pp. 1971–1976, doi: 10.1109/PVSC43889.2021.9518628.

[6] A. Jain, W.-J. J. Choi, Y.-Y. Y. Huang, B. Klein, and A. Rohatgi, “Design, optimization, and in-depth understanding of front and rear junction double-side passivated contacts solar cells,” *IEEE J. Photovolt.*, vol. 11, no. 5, pp. 1141–1148, Sep. 2021, doi: 10.1109/JPHOTOV.2021.3086461.

[7] A. Ingenito et al., “Silicon solar cell architecture with front selective and rear full area ion-implanted passivating contacts,” *Sol. RRL*, vol. 1, no. 7, 2017, Art. no. 1700040, doi: 10.1002/solr.201700040.

[8] K. Chen et al., “Self-aligned selective area front contacts on poly -Si/SiOx passivating contact c-Si solar cells,” *IEEE J. Photovolt.*, vol. 12, no. 3, pp. 678–689, May 2022, doi: 10.1109/JPHOTOV.2022.3148719.

[9] S. Schäfer et al., “Laser-induced modification of doped poly-si surface for si solar cells with structured passivated contacts,” in *Proc. 37th Eur. Photovolt. Sol. Energy Conf.*, 2020, pp. 37–39. doi: 10.4229/EU-PVSEC20202020-2DV.3.5.

[10] S. Schäfer et al., “Role of oxygen in the UV-ps laser triggered amorphization of poly-SI for SI solar cells with local passivated contacts,” *J. Appl. Phys.*, vol. 129, no. 13, Apr. 2021, Art. no. 133103, doi: 10.1063/5.0045829.

[11] T. Matsumoto, H. Tsuji, S. Terakawa, and H. Kobayashi, “Ultra-low power poly-SI TFTs with 10 nm stacked gate oxide fabricated by nitric acid oxidation of silicon (NAOS) method,” *ECS J. Solid State Sci. Technol.*, vol. 4, no. 5, pp. N36–N40, 2015, doi: 10.1149/2.0151505jss.

[12] G. E. Jellison and F. A. Modine, “Parameterization of the optical functions of amorphous materials in the interband region,” *Appl. Phys. Lett.*, vol. 69, no. 3, pp. 371–373, Jul. 1996, doi: 10.1063/1.118064.

[13] T. E. Tiwald, D. W. Thompson, J. A. Woollam, W. Paulson, and R. Hance, "Application of IR variable angle spectroscopic ellipsometry to the determination of free carrier concentration depth profiles," *Thin Solid Films*, vol. 313–314, pp. 661–666, Feb. 1998, doi: 10.1016/S0040-6090(97)00973-5.

[14] P. Padhamnath et al., "Optoelectrical properties of high-performance low-pressure chemical vapor deposited phosphorus-doped polysilicon layers for passivating contact solar cells," *Thin Solid Films*, vol. 699, 2020, Art. no. 137886, doi: 10.1016/j.tsf.2020.137886.

[15] S. C. Baker-Finch and K. R. McIntosh, "A freeware program for precise optical analysis of the front surface of a solar cell," in *Proc. 35th IEEE Photovolt. Specialists Conf.*, 2010, pp. 002184–002187, doi: 10.1109/PVSC.2010.5616132.

[16] K. R. McIntosh and S. C. Baker-Finch, "OPAL 2: Rapid optical simulation of silicon solar cells," in *Proc. 38th IEEE Photovolt. Specialists Conf.*, 2012, pp. 265–271, doi: 10.1109/PVSC.2012.6317616.

[17] D. S. Jensen et al., "Silicon (100)/SiO_2 by XPS," *Surf. Sci. Spectra*, vol. 20, no. 1, pp. 36–42, Dec. 2013, doi: 10.1116/11.20121101.

[18] H. P. Ma et al., "Systematic study of the SiOx film with different stoichiometry by plasma-enhanced atomic layer deposition and its application in SiOx/SiO_2 super-lattice," *Nanomaterials*, vol. 9, no. 1, pp. 1–13, 2019, doi: 10.3390/nano9010055.

[19] T. E. Orlowski and D. A. Mantell, "Ultraviolet laser-induced oxidation of silicon: The effect of oxygen photodissociation upon oxide growth kinetics," *J. Appl. Phys.,* vol. 64, no. 9, 1988, Art. no. 4410, doi: 10.1063/1.341263.

[20] J. Yoo, J. So, G. Yu, and J. Yi, "Study on hydrogenated silicon nitride for application of high efficiency crystalline silicon solar cells," *Sol. Energy Mater. Sol. Cells*, vol. 95, no. 1, pp. 7–10, Jan. 2011, doi: 10.1016/J.SOLMAT.2010.03.031.

[21] A. Fell, K. R. McIntosh, M. Abbott, and D. Walter, "Quokka version 2: Selective surface doping, luminescence modeling and data fitting," 2013. [Online]. Available: https://downloads.pvlighthouse.com.au/Quokka2/fell2013-quokka2-pvsec-23.pdf

[22] T. N. D. Tibbits et al., "GridTOUCH: Innovative solution for accurate IV measurement of busbarless cells in production and laboratory environments," in *Proc. 29th Eur. Photovolt. Sol. Energy Conf. Exhib.*, 2014, pp. 1180–1185, doi: 10.4229/EUPVSEC20142014-2BV.8.24.

[23] K. Madani et al., "Comparison of passivation properties of plasma-assisted ALD and APCVD deposited Al2O3 with sinx capping," *Sol. Energy Mater. Sol. Cells*, vol. 218, 2020, Art. no. 110718, doi: 10.1016/j.solmat.2020.110718.

[24] W.-J. J. Choi, A. Jain, Y.-Y. Y. Huang, Y.-W. W. Ok, and A. Rohatgi, "Quantitative understanding and implementation of screen printed P+ Poly-Si/Oxide passivated contact to enhance the efficiency of P-PERC cells," in *Proc. IEEE Photovolt. Specialists Conf.*, 2020, pp. 0821–0824. doi: 10.1109/PVSC45281.2020.9300878.

[25] Y.-Y. Huang et al., "Fully screen-printed bifacial large area 22.6% N-type si solar cell with lightly doped ion-implanted boron emitter and tunnel oxide passivated rear contact," *Sol. Energy Mater. Sol. Cells*, vol. 214, Aug. 2020, Art. no. 110585, doi: 10.1016/j.solmat.2020.110585.

[26] Y.-Y. Y. Huang et al., "$\sim$23% rear side poly-Si/SiO2 passivated silicon solar cell with optimized ion-implanted boron emitter and screen-printed contacts," *Sol. Energy Mater. Sol. Cells*, vol. 230, Sep. 2021, Art. no. 111183, doi: 10.1016/j.solmat.2021.111183.

[27] M. R. Payo et al., "LPCVD polysilicon-based passivating contacts for plated bifacial n-Type PERT solar cells," in *Proc. 35th Eur. Photovolt. Sol. Energy Conf. Exhib.*, 2018. [Online]. Available: https://www.eupvsec-proceedings.com/proceedings?paper=46557